Quantum scattering studies of electronically inelastic collisions of N+ 2(X 2Σ+ g , A 2Π u) with He

Andreas Berning and HansJoachim Werner

Citation: The Journal of Chemical Physics **100**, 1953 (1994); doi: 10.1063/1.466548
View online: http://dx.doi.org/10.1063/1.466548
View Table of Contents: http://scitation.aip.org/content/aip/journal/jcp/100/3?ver=pdfcov
Published by the AIP Publishing

Quantum scattering studies of electronically inelastic collisions of $N_2^+(X\,^2\Sigma_g^+,\ A\,^2\Pi_u)$ with He

Andreas Berning and Hans-Joachim Werner
Fakultät für Chemie, Universität Bielefeld, 33615 Bielefeld, Germany

(Received 3 September 1993; accepted 12 October 1993)

The potential energy surfaces (PESs) of the three lowest electronic states of the system $N_2^+ + He$ have been computed using accurate multiconfiguration-reference configuration (MRCI) wave functions and a large basis set. The approach of the He atom leads to nonadiabatic mixing of the $A\,^2\Pi_u(A')$ and $X\,^2\Sigma_g^+(A')$ states of N_2^+. The three adiabatic interaction potentials have been transformed into a set of four diabatic potentials, one of which describes the collision-induced nonadiabatic coupling between the two A' states. The computed potentials have been fitted to analytical functions and used in quantum scattering calculations for electronically inelastic transitions between individual rovibrational levels of the $A\,^2\Pi_u$ and the $X\,^2\Sigma_g^+$ states of N_2^+. Our results are compared to transitions observed experimentally by Katayama and co-workers between the rotational levels of the $A,v=3$ and 4 and $X,v=6$, 7, and 8 vibrational manifolds. In general, good agreement is found for transitions between nearly isoenergetic vibrational states. However, for transitions which traverse large energy gaps, we obtained cross sections which are several orders of magnitude smaller than experimentally observed. Inclusion of the vibrational degree of freedom of the N_2^+ molecule in the scattering calculations was found to have only an insignificant effect on the transition probabilities.

I. INTRODUCTION

In the past decade, there have been numerous experimental studies on the collisional quenching of electronically excited diatomic molecules, but only relatively few in which the initial and final states were monitored directly with fine-structure resolution. Katayama and co-workers[1–10] investigated transfer processes from the $A\,^2\Pi$ to the $X\,^2\Sigma^+$ states in N_2^+ and CO^+ with He as a collision partner using an optical–optical double resonance technique. Dagdigian and co-workers[11–14] performed analogous experiments for CN+Ar and, very recently, for CN +He.[15] These experiments showed that collision-induced energy transfer between different electronic states can be of similar magnitude as rotational energy transfer in a single electronic state.

Since in the Born–Oppenheimer approximation any couplings between different electronic states are absent, nonadiabatic effects must be responsible for the observed transitions. Early theoretical work assumed non-Born–Oppenheimer coupling between different electronic states in the *isolated* molecule to be the origin of the collision-induced electronic energy transfer.[16–19] However, since in the N_2^+ molecule the two concerned electronic states $A\,^2\Pi_u$ and $X\,^2\Sigma_g^+$ have different *permutation–inversion* symmetry, non-Born–Oppenheimer perturbations are absent in the isolated molecule,[20] and this *gateway mechanism* cannot explain the observed transitions. Alexander and Corey[21] proposed that nonadiabatic Σ–Π mixing is induced by the approach of the rare gas atom, which can lead to collision-induced electronic transitions even in the absence of nonadiabatic coupling in the isolated molecule. They developed a formal theory for the quantum scattering treatment of collision-induced transitions between $^2\Sigma$ and $^2\Pi$ electronic states, which was later applied to the $CN(A\,^2\Pi,\ X\,^2\Sigma^+)$+He system by Werner and co-workers.[22,23] The scattering calculations,[23] which were based on *ab initio* potential energy surfaces,[22] yielded cross sections in good agreement with the experiments of Dagdigian *et al.*[11–14] In particular, the experimentally observed propensity for small changes of the rotational quantum number ($\Delta J \approx 0$), even for transitions between off-resonant vibrational levels in the X and A states, as well as pronounced alternations between final rotational states with even and odd J, could be nicely reproduced and explained. In a recent reinvestigation for the CN+He system,[15] nonadiabatic perturbations in the isolated CN molecule were also taken into account. It was shown that the gateway mechanism based on such couplings can in certain cases lead to significantly enlarged cross sections, but is in general not the dominant mechanism and not able to explain the details of the experimental results.

Both Dagdigian *et al.*[11–14] and Katayama *et al.*[5,6,9] observed transitions between energetically nearly degenerate as well as "out-of-resonance" vibrational levels of the X and A states of CN and N_2^+, respectively. Surprisingly, the large energy gap transitions were found to be almost as strong as the nearly isoenergetic ones. For instance, Katayama *et al.* observed efficient transitions from the $A,v=3(4)$ state to the $X,v=6(7)$ states, which are separated by energy gaps of 1750 to 2000 cm^{-1} (see Fig. 1).

However, theory so far failed to reproduce the magnitude of cross sections for transitions with large energy gaps. For the CN+He system, the calculated cross sections for the $A,v=3\rightarrow X,v=7$ transitions, which have an energy gap of about 600 cm^{-1}, were found to be three to four orders of magnitude smaller than those for the $A,v=7\rightarrow X,v=11$ transitions, which have a very small energy gap. In the present paper, we present new calculations for the isoelectronic N_2^+ +He system. This system was chosen

 0021-9606/94/100(3)/1953/15/$6.00

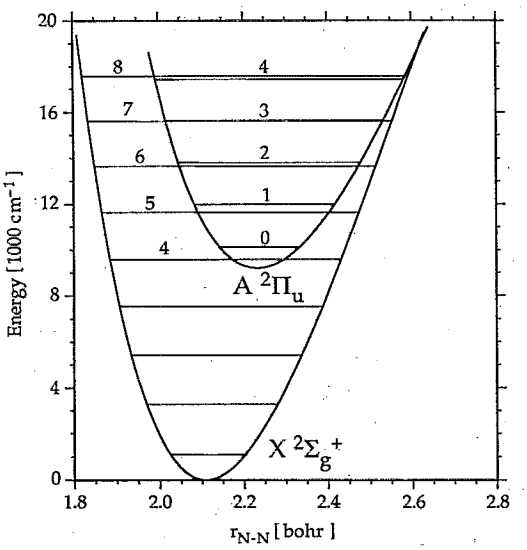

FIG. 1. Potential energy curves and vibrational energies (referred to the bottom of the X state potential well) for the ground state $X\,^2\Sigma_g^+$ and first excited state $A\,^2\Pi_u$ of N_2^+.

for several reasons. First, as already mentioned, nonadiabatic interactions in the isolated molecule are absent due to symmetry reasons and pose no complications. Second, due to the charge–induced dipole interaction, the attractive wells are considerably deeper than for CN+He, and it is of interest to investigate whether this has an effect on the collision-induced electronic energy transfer. Third, due to the dominant electrostatic nature of the atom–ion interaction, the computed *ab initio* potentials are expected to be more accurate than for CN+He, since weak dispersion forces are of less importance. This largely eliminates the question of whether errors in the *ab initio* potentials could be responsible for the failure of the calculations to reproduce the large energy gap transition probabilities. Finally, in the present paper, we address the question whether inclusion of the N_2^+ vibrational motion in the scattering treatment is of importance. In our previous calculations[15,22,23] for CN+He, this degree of freedom was neglected (rigid-rotor approximation), which might not be justified for transitions between off-resonant vibrational levels.

The present paper is organized as follows: in Sec. II, we describe details of the *ab initio* calculations of the three-dimensional potential energy surfaces (PESs) needed for the scattering calculations. The *adiabatic* PESs are obtained using accurate multireference configuration expansions. The adiabatic mixing between the two A' states is derived by inspection of the adiabatic wave functions, under the assumption that no orbital mixing occurs, and used to transform to the *diabatic* representation. This approximation has been found to be very accurate in our previous *ab initio* calculations for CN+He.[22] In Sec. III, we describe the resulting *adiabatic* and *diabatic* potential energy surfaces. Section IV briefly reviews some aspects of the underlying scattering theory with a discussion of the particular case of a homonuclear molecule+atom system. The results of the scattering calculations are analyzed and discussed in Sec. V. The paper concludes with a short summary.

II. *AB INITIO* CALCULATIONS

The interaction potential energy surface of the system N_2^++He is a function of three coordinates: R is the distance of the helium atom from the center of mass of N_2^+, r is the bond length of the N_2^+ molecule, and θ is the angle between **R** and **r**. The N_2^+ bond defines the z axis and the N_2^++He system lies in the xz plane.

All *ab initio* calculations were performed with the MOLPRO program.[24] In order to obtain reliable interaction potentials, it is necessary to employ highly correlated electronic wave functions and large atomic basis sets. In this section, we will first describe the one-electron atomic orbital (AO) basis sets, second the N-electron basis sets, and finally the transformation of the energies to a diabatic representation.

In the present case, the long-range part of the potential is dominated by the inductive interaction of the charge of the N_2^+ fragment with the dipole polarizability of the He atom. Smaller contributions come from the interaction of the induced dipole in He with the dipole and quadrupole polarizabilities of N_2^+. The computation of reliable polarizabilities requires flexible s, p basis sets and the inclusion of diffuse d and f polarization functions. In order to keep the basis set size reasonably small, the exponents of the d and f functions were optimized to reproduce as accurately as possible the dipole and quadrupole polarizabilities of the fragments as obtained with considerably larger basis sets. For the helium atom, we used the Huzinaga 8s Gaussian basis set[25,26] with the first four functions contracted; this basis was augmented by three p functions with exponents 1.2, 0.4, and 0.13 (all exponents in bohr^{-2}) and two d functions with exponents 0.8 and 0.25. The basis for nitrogen was based on the 13s8p set of van Duijneveldt,[27] which was contracted to [7s5p] and expanded by three d functions with exponents 2.2, 0.66, and 0.22 as well as two f functions with exponents 1.093 and 0.35.

In Tables I and II, we compare the calculated multipole moments and polarizabilities for the helium atom in the electronic ground state (^1S) and the N_2^+ molecule in the first excited state ($A\,^2\Pi_u$) for different basis sets. A definition of all quantities can be found in Ref. 28. All values were obtained as first and second derivatives of the energy with respect to finite electric fields F_α and field gradients $F_{\alpha\beta}$. In these test calculations, the energies of He and N_2^+ have been calculated using the full configuration interaction (FCI) and coupled electron pair approximation (CEPA)[29,30] methods, respectively. In both tables, basis A is the one described above, which was used for the final calculations, while sets B and C are larger and more flexible. Table I shows that the basis A slightly overestimates dipole polarizability of He and underestimates the quadrupole polarizability, as compared to calculations with larger basis sets. However, as also shown in Table I, these errors have only a very small effect on the N_2^++He interaction energies at long range. As demonstrated in Ta-

TABLE I. Dipole (α) and quadrupole (C) polarizabilities of helium, and N_2^+ ($A\,^2\Pi_{u,y}$)–He interaction energies for different He basis sets.

Basis[a]	α	C	$V_\parallel$ [b]	$V_\perp$ [c]
A	1.3970	2.2234	−85.40	−138.03
B	1.3969	2.4700	−85.49	−138.15
C	1.3844	2.4473	−84.68	−138.40
Previous calculation[d]	1.3831	2.4434		
Experiment[e]	1.3860±0.0051			

[a]For the N_2^+ molecule, the basis A from Table II has been used. Interaction energies are given in cm^{-1}; all other values in atomic units. Basis A: final basis set (see the text); basis B: basis A with three d (0.8, 0.31, and 0.105) functions; basis C: Huzinaga 10s+"even tempered" p, d, and f functions, $\eta_i = C \cdot X^{(n+1)/2-i}$ with $n_p=10$, $C_p=0.4$, $X_p=2$, $n_d=6$, $C_d=0.45$, $X_d=3$, $n_f=3$, $C_f=0.5$, and $X_f=3$, respectively.
[b]$V_\parallel$ denotes the interaction energy for $r=2.11$ bohr, $R=7.0$ bohr, and $\theta=0°$.
[c]$V_\perp$ denotes the interaction energy for $r=2.11$ bohr, $R=6.0$ bohr, and $\theta=90°$.
[d]Reference 31.
[e]Reference 32.

ble II, the quadrupole moment and the dipole polarizabilities of the $A\,^2\Pi_{u,y}$ state of N_2^+ are even less sensitive to the choice of the polarization functions, and the N_2^++He interaction energies are hardly affected. We therefore believe that our basis set yields a result quite close to the basis set limit.

We now turn to the description of the electron correlation treatment. As zeroth order approximations for the N-electron wave functions, we used state-averaged complete active space self-consistent field (CASSCF) wave functions.[34–37] The orbitals and configuration expansion coefficients were obtained by minimizing the energy average of the lowest two A' and one A'' states; these states correlate asymptotically with the $A\,^2\Pi$ and $X\,^2\Sigma^+$ states of N_2^++He. In all configurations of the CASSCF wave functions, the $1a'$ and $2a'$ orbitals (nitrogen 1s) and the $3a'$ orbital (helium 1s) were doubly occupied. The active orbital space comprised the $4a'$–$9a'$, $1a''$, and $2a''$ orbitals, leading to a total of 1204 and 1148 configuration state functions (CSFs) for A' and A'' symmetries, respectively. Asymptotically the active orbitals correlate with the $2\sigma_g$, $3\sigma_g$, $2\sigma_u$, $3\sigma_u$, $1\pi_u$, and $1\pi_g$ valence orbitals of N_2^+. The optimized active orbitals were transformed to state-averaged natural orbitals, which diagonalize the state-averaged first order density matrix. The inactive orbitals were transformed to a pseudocanonical representation, which diagonalizes the corresponding blocks of an effective Fock operator.

The above procedure yielded a single set of uniquely defined orbitals for all states which was used in subsequent internally contracted multireference configuration interaction (MRCI) calculations.[38,39] In the MRCI, all single and double excitations from the reference configurations were taken into account, and all electrons except for those occupying the $1a'$ and $2a'$ core orbitals were correlated. Since the computational effort for the MRCI with the above CASSCF reference wave functions is quite large, we restricted the reference space by only allowing configurations in the reference wave function which have a maximum of two electrons in the weakly occupied $8a'$, $9a'$, and $2a''$ orbitals. Furthermore, no excitations from the 4σ orbital were allowed in the reference wave functions. Test calculations for various geometries showed that these approximations influence the computed interaction energies by no more than 5%. The resulting restricted reference space (RAS) consisted of 246 CSFs of A' and 224 CSFs of A'' symmetry. With the atomic orbital (AO) basis used in the final calculations (see below), the MRCI wave functions included a total of 21 297 143 (20 976 755) uncontracted CSFs and 691 179 (675 941) variational parameters for the A' (A'') symmetries, respectively.

Each electronic state was computed separately with one reference state. In order to avoid root flipping during the optimization of the $2A'$ state, an approximate projection technique[40] was employed, and the resulting two slightly nonorthogonal A' wave functions were used as a basis in a final 2×2 variational calculation. Alternatively, one can use more extended wave functions, in which the direct sum of the contracted $1A'$ and $2A'$ configuration spaces is used as a basis for both states (two reference states). It was found that the interaction energies obtained with the one- and two-reference state treatments differ typically by only 1%. The one reference state treatment yields accurate results even in the region of the conical intersection of the $1A'$ and $2A'$ surfaces, which occurs at extended N_2^+ distances. Therefore, the computationally less de-

TABLE II. Calculated quadrupole moments, dipole polarizabilities of N_2^+ ($A\,^2\Pi_u$), and interaction energies for N_2^+ ($A\,^2\Pi_{u,y}$)+He using various basis sets.[a]

Basis[b]	Q	$\alpha_\parallel$	$\alpha_\perp$	$V_\parallel$ [c]	$V_\perp$ [d]
A	−0.1445	10.707	6.248	−85.40	−138.03
B	−0.1444	10.712	6.269	−85.81	−138.52
C	−0.1390	10.715	6.458	−86.33	−139.09
D	−0.1426	10.706	6.288	−86.91	−139.67

[a]Q is the quadrupole moment along the molecular axis, and $\alpha_\parallel$ and $\alpha_\perp$ are the dipole polarizabilities along and perpendicular to the molecular axis, respectively. The bond distance is 2.11 bohr, interaction energies are in cm^{-1}, and all other values are in atomic units.
[b]For the He atom, the basis A from Table I has been used. Basis A: final basis set (see the text); basis B: basis A with additional diffuse d (0.073) and f (0.12) functions; basis C: $AVQZ$ [6s5p4d3f2g] (see Ref. 33); basis D: $AV5Z$ [7s6p5d4f3g] (see Ref. 33).
[c]$V_\parallel$ denotes the interaction energy for $r=2.11$ bohr, $R=7.0$ bohr, and $\theta=0°$.
[d]$V_\perp$ denotes the interaction energy for $r=2.11$ bohr, $R=6.0$ bohr, and $\theta=90°$.

TABLE III. Adiabatic interaction energies[a] for $N_2^+(X\,^2\Sigma_g^+, A\,^2\Pi_{u,y})$–He($X\,^1S$) using various electron correlation treatments.

R	MRCI (72/4)[c]	MRCI (82/4)[d]	MRCI+Q[e] (72/4)	ACPF[f] (72/4)	CEPA(1)[g]	ΔE_{CP}[h]
			$^2\Sigma^+$			
50.0	(776.55)[b]	(496.15)	(37.12)	(33.20)		
7.0	−100.88	−103.09	−107.21	−106.59		5.06
6.0	−133.35	−136.16	−151.77	−148.33		9.83
5.0	461.13	475.11	384.40	413.32		27.18
			$^2\Pi$			
50.0	(728.21)	(434.78)	(23.63)	(3.70)	(0.0)	
7.0	−72.55	−74.46	−77.68	−77.14	−85.40	5.72
6.0	6.70	3.26	−5.50	−3.83	−15.37	11.05
5.0	1453.56	1461.13	1423.37	1428.54	1383.84	29.72

[a]All energies are given in cm^{-1} and are counterpoise and size consistency corrected; r=2.11 bohr, and θ=0°.
[b]Values in parentheses are size consistency errors for R=50 bohr.
[c]MRCI(72/4) denotes a reference space with seven σ and two π orbitals; the lowest four σ orbtals are closed shells in the reference. The lowest two σ core orbitals are not correlated. Occupancy restrictions for the 7σ, (8σ), and 2π orbitals have been imposed in all cases as described in the text.
[d]The additional 8σ orbital correlates asymptotically with He ($3s$).
[e]The same as footnote c, but with the Davidson correction (Ref. 43) for the effect of unlinked cluster effects.
[f]The internally contracted multireference averaged coupled pair functional see Refs. 44 and 45).
[g]Single-reference coupled electron pair approximation (see Ref. 30).
[h]Counterpoise corrections for MRCI(72/4).

manding single state technique has been used for all final calculations.

A disadvantage of the variational MRCI method for calculating interaction energies is its lack of size consistency, i.e., the computed energy for the N_2^+ + He system at infinite separation is not the sum of the separately computed N_2^+ and He energies. The size consistency error ΔE_{sc} can be accounted for by assuming it is independent with respect to R and θ and equals the interaction energy at infinite distance (R=50 bohr in the actual calculations)

$$\Delta E_{sc}(r) = E_{N_2^+ + He}(\infty, r) - E_{N_2^+}(\infty, r) - E_{He}(\infty), \quad (1)$$

where $E_{N_2^+ + He}(\infty, r)$ is the total energy of the complex at infinite distance R, and $E_{N_2^+}(\infty, r)$ and $E_{He}(\infty)$ are the separately calculated fragment energies. ΔE_{sc} is subtracted from the computed interaction energies at each geometry. Due to the incompleteness of the basis sets, one also has to correct for basis superposition errors (BSSEs), which is done by applying the counterpoise correction (CPC) proposed by Boys and Bernardi.[41] For the N_2^+ + He system, the CPC is defined by

$$\Delta E_{CP}(R,\theta,r) = E_{N_2^+}(\infty, r) - E_{N_2^+}(R,\theta,r) + E_{He}(\infty) - E_{He}(R,\theta,r), \quad (2)$$

where $E_{N_2^+}(R,\theta,r)$ and $E_{He}(R,\theta,r)$ are the energies obtained in computations with the additional basis functions of the other fragment at the positions defined by R and θ. Since both the size consistency and counterpoise corrections are different for the three electronic states of interest, they have to be applied separately to each of the states. The total interaction energy finally takes the form

$$V(R,\theta,r) = E_{N_2^+ + He}(R,\theta,r) - E_{N_2^+}(R,\theta,r) - E_{He}(R,\theta,r) - \Delta E_{sc}(r), \quad (3)$$

where $E_{N_2^+ + He}(R,\theta,r)$ denotes the *diabatic* energy of the complex at the specified geometry as defined later in this section.

In order to study the effect of various approximations in the correlation treatment, we computed the interaction energies at a number of geometries using various methods and active orbital spaces. A subset of these results is shown in Table III. The results in the first column of this table were obtained with the wave functions as described above. In the second column, we have included excitations from the He $2s$ into the He $3s$ orbital in the reference wave functions. This reduces the size consistency error almost by a factor of 2, which is due to the effective inclusion of additional triple and quadruple excitations relative to the full valence CASSCF reference functions; such configurations are known to be important for the accurate prediction of dispersion energies[42] and therefore increase the long-range attraction. The unlinked cluster effects of higher excitations can also be accounted for approximately in non-variational variants of the MRCI method. Table III shows results obtained with Davidson corrected energies[43] (MRCI+Q) and with the internally contracted multireference averaged coupled pair approximation[44,45] (MR-ACPF). Both methods yield much smaller size consistency errors and slightly more attractive interaction potentials than the variational MRCI. Finally, for the $A\,^2\Pi$ state, also CEPA results are shown. This single reference method[29,30] has been found previously to give quite accurate interaction potentials for OH($X\,^2\Pi$,$A\,^2\Sigma^+$) + He, Ar.[46,47] For the present case, it yields potentials which are in the long-range part 10%–15% more attractive than the MRCI and MR-ACPF ones. The various multireference treatments yields well depths which differ only by about 5%. Even though the present calculations do not allow a definite conclusion about which results are most accurate, we feel that the overall errors in our correlation treatment should be

fairly small. Finally, we note that the counterpoise corrections are also quite small, as demonstrated in the last column of Table III.

As described in earlier papers,[22,23] we assume that the approach of the helium atom to the N_2^+ molecule mixes only the $A\,^2\Pi_u$ and $X\,^2\Sigma_g^+$ states of the diatom. The degenerate pair of wave functions of N_2^+ in the $A\,^2\Pi_u$ state are chosen to be $|\Pi_x\rangle$, which is symmetric (A'), and $|\Pi_y\rangle$, which is antisymmetric (A'') with respect to reflection of the spatial coordinates in the triatomic plane. With decreasing N_2^+–He distances at nonlinear geometries, the $\Pi_x(A')$ wave function becomes mixed with the wave function correlating asymptotically to $N_2^+(X\,^2\Sigma_g^+)+$He, which has also A' symmetry. Therefore the resulting *adiabatic* electronic wave functions for the two lowest states of A' symmetry can be written approximately as

$$\psi_1(R,\theta,r)=\cos\chi|\Sigma^+\rangle-\sin\chi|\Pi_x\rangle, \tag{4}$$

$$\psi_2(R,\theta,r)=\sin\chi|\Sigma^+\rangle+\cos\chi|\Pi_x\rangle, \tag{5}$$

where $|\Sigma^+\rangle$ and $|\Pi_x\rangle$ represent *diabatic* electronic wave functions and χ is the *adiabatic* mixing angle. The matrix elements of the electronic Hamiltonian in the *diabatic* basis as well as the mixing angle χ are functions of the three internal coordinates R, r, and θ. Neglecting non-Born–Oppenheimer spin–orbit and spin–rotation coupling in the $^2\Sigma$ and $^2\Pi$ states, the angular dependence of these four matrix elements can be expanded as[21]

$$\langle\Sigma^+|H_{el}|\Sigma^+\rangle\equiv T_\Sigma(r)+V_\Sigma(R,r,\theta)$$
$$=T_\Sigma(r)+\sum_{l=0}^{\infty}V_\Sigma^l(R,r)d_{00}^l(\theta), \tag{6}$$

$$\langle\Pi_{x,y}|H_{el}|\Pi_{x,y}\rangle\equiv T_\Pi(r)+V_\Pi(R,r,\theta)\mp V_2(R,r,\theta)$$
$$=T_\Pi(r)+\sum_{l=0}^{\infty}V_\Pi^l(R,r)d_{00}^l(\theta)$$
$$\mp\sum_{l=2}^{\infty}V_2^l(R,r)d_{20}^l(\theta), \tag{7}$$

$$\langle\Sigma^+|H_{el}|\Pi_x\rangle\equiv\langle\Pi_x|H_{el}|\Sigma^+\rangle$$
$$=V_1(R,r,\theta)$$
$$=\sqrt{2}\sum_{l=1}^{\infty}V_1^l(R,r)d_{10}^l(\theta). \tag{8}$$

The terms $T_\Sigma(r)$ and $T_\Pi(r)$ in Eqs. (6) and (7) are the potential energy functions of the $^2\Sigma$ and $^2\Pi$ states in the isolated N_2^+ molecule, whereas the diabatic interaction potentials $V_\Sigma(R,r,\theta)$, $V_\Pi(R,r,\theta)$, $V_1(R,r,\theta)$, and $V_2(R,r,\theta)$ describe the change in the electronic Hamiltonian due to the approach of the collision partner. Here d_{mn}^l are reduced rotation matrix elements,[48] and in Eq. (7), the minus sign belongs to the V_{Π_x} potential.

Labeling the energies of the two *adiabatic* states of A' symmetry, which correlate at large distances R with $N_2^+(X\,^2\Sigma_g^+)+$He and $N_2^+(A\,^2\Pi_u)+$He, with $E_1=\langle\Psi_1|H_{el}|\Psi_1\rangle$ and $E_2=\langle\Psi_2|H_{el}|\Psi_2\rangle$, respectively, and the energy of the state of A'' symmetry, which also correlates asymptotically with $N_2^+(A\,^2\Pi_u)+$He, with $E_3=\langle\Psi_3|H_{el}|\Psi_3\rangle$, one obtains the following relations among the four *diabatic* potentials V_Σ, V_Π, V_1, and V_2 and the three *adiabatic* energies E_1, E_2, and E_3 for each R, r, and θ:

$$V_\Sigma=E_1\cos^2\chi+E_2\sin^2\chi, \tag{9}$$

$$V_\Pi=\tfrac{1}{2}(E_1\sin^2\chi+E_2\cos^2\chi+E_3), \tag{10}$$

$$V_1=\tfrac{1}{2}(E_1-E_2)\sin 2\chi, \tag{11}$$

$$V_2=\tfrac{1}{2}(-E_1\sin^2\chi-E_2\cos^2\chi+E_3). \tag{12}$$

At large distances R or collinear geometries, the mixing angle χ goes to zero, E_2 becomes equal to E_3, and both V_1 and V_2 vanish.

The *adiabatic* mixing angle χ between the $X\,^2\Sigma_g^+$ and $A\,^2\Pi_{u,x}$ states, which in the presence of the He atom are both of A' symmetry, has been obtained by inspection of the coefficients of the configuration expansion in the MRCI wave functions.[22] This method assumes that the approach of the He atom does not lead to a nonadiabatic mixing of the active orbitals, which is well justified for the state-averaged natural orbitals as described above. In our previous similar calculations for the isoelectronic CN+He system, we found that this simple method yields virtually identical results as a more complicated procedure involving the computation and integration of nonadiabatic coupling matrix elements.[22]

III. POTENTIAL ENERGY SURFACES

Interaction energies for the N_2^++He system have been calculated for a large number of geometries. To describe the angular dependence of the potentials properly, we performed calculations for four different angles θ, namely, 0°, 30°, 60°, and 90°, which is due to the symmetry of N_2^+, equivalent to spanning the angular range of the potential by a grid of seven points. The vibrational motion of the N_2^+ molecule is accounted for by calculating interactions energies for three different bond distances r, namely, 1.90, 2.11, and 2.65 bohr, which cover the region of the classical turning points of the diatom for the vibrational states under investigation in the subsequent scattering calculations. For each angle θ and bond distance r, the potentials have been calculated for 11–13 R values in the range from 3.0 to 11.0 bohr. The potential energy surfaces are available from the authors on request.

The computed energies were transformed to the diabatic representation as described in Sec. II. The four resulting potential energy functions V_Σ, V_Π, V_1, and V_2 were then fitted to functions of the form

$$V_i(R,r,\theta)=\sum_l A_{ln}^i(R)d_{l0}^l(\theta)(r-r_e)^n. \tag{13}$$

Details about this fitting procedure and the functional form of the coefficients $A_{ln}^i(R)$ can be found in Ref. 22.

The r dependence of these potentials was represented in the basis of vibrational wave functions $\chi_v(r)$ of the iso-

TABLE IV. Spectroscopic constants of the $X\,^2\Sigma_g^+$ and $A\,^2\Pi_u$ states of the N_2^+ molecule.

State	Method	r_e[a]	B_e[b]	α_e[b]	ω_e[b]	$\omega_e x_e$[b]
$X\,^2\Sigma_g^+$	CMRCI	2.1166	1.919	0.0185	2193.4	15.8
	Expt.[c]	2.1097	1.932	0.0190	2207.0	16.1
$A\,^2\Pi_u$	CMRCI	2.2263	1.735	0.0185	1898.0	15.3
	Expt.[c]	2.2179	1.748	0.0200	1903.5	15.0

[a]In bohr.
[b]In cm^{-1}.
[c]Reference 50.

lated N_2^+ molecule. The necessary vibrational matrix elements of the interaction potentials take the form

$$V_l^{v',v}(R,\theta)=\sum_l A_{ln}^i(R)d_{i0}^l(\theta)\langle\chi_{v'}|(r-r_e)^n|\chi_v\rangle. \quad (14)$$

Since the Rydberg–Klein–Rees (RKR) data[49,50] for the two lowest electronic states of N_2^+ are not complete, we calculated accurate potential energy curves for the $X\,^2\Sigma_g^+$ and the $A\,^2\Pi_u$ states using full-valence CASSCF-MRCI wave functions and a [6*s*5*p*3*d*2*f*1*g*] basis set.[33] From the resulting potentials, equilibrium geometries and other spectroscopic properties have been derived which are in excellent agreement with experimental data (see Table IV). The vibrationally averaged matrix elements $\langle\chi_{v'}|(r-r_e)^n|\chi_v\rangle$ were determined by numerical quadrature of the corresponding vibrational wave functions obtained by Numerov integration.[51]

The general features of the *adiabatic* potentials energy surfaces can be deduced from the dominant electron configurations of the X and A states of N_2^+ at its equilibrium distance. The $X\,^2\Sigma_g^+(A')$ state is $(1\sigma-4\sigma)^8(\equiv\text{core})$ $5\sigma^1\pi_x^2\pi_y^2$, the $A\,^2\Pi_{u,x}(A')$ state is core $5\sigma^2\pi_x^1\pi_y^2$, and the $A\,^2\Pi_{u,y}(A'')$ state is core $5\sigma^2\pi_x^2\pi_y^1$. This implies that at collinear geometries, the $^2\Pi_u$ states with a doubly occupied 5σ orbital are more repulsive than the $^2\Sigma_g^+$ state. On the other hand, for the perpendicular ($\theta=90°$) approach, the states with a doubly occupied π_x orbital, namely, $^2\Sigma_g^+$ and $^2\Pi_{u,y}$, are more repulsive than the $^2\Pi_{u,x}$ state. These features can be seen in the contour plots of the three *adiabatic* potential energy surfaces in Figs. 2–4.

The effect of a variation of the N_2^+ bond distance on the diabatic interaction potential energy surfaces differs depending on the electronic state under consideration (Table V). The qualitative shape of the interaction potentials for the two $^2\Pi_u$ states is independent of r, but the minima become less deep and shift to larger R with increasing r. The influence on the $^2\Pi_{u,x}$ potential is larger than for the $^2\Pi_{u,y}$ state. In contrast, the topology of the $^2\Sigma_g^+$ surface changes qualitatively with increasing r. The minimum for $r=1.90$ bohr is at $\theta=90°$, whereas for the stretched N_2^+ ($r=2.65$ bohr), the minimum is located at collinear geometry. The influence of r on the depth of the potential well of the $^2\Sigma_g^+$ state is less pronounced than for the $^2\Pi_{u,x}$ state. In order to check whether the fitted r dependence of the potentials is reasonable, we performed some additional calculations for $r=2.40$ bohr. The agreement between the interpolated and calculated points was satisfactory, and cuts through the potential energy surfaces showed that no artificial extrema had been introduced by the fitting procedure.

Figures 5, 6, and 7 show some cuts through the four

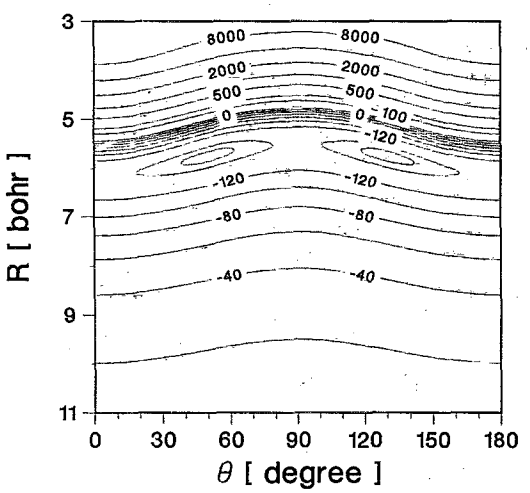

FIG. 2. Contour plot of the *adiabatic* potential energy surface of $N_2^+(X\,^2\Sigma_g^+)+He$; $r=2.11$ bohr. Lines are drawn at -144 and -140 cm^{-1}, every 20 cm^{-1} in the range from -120 to 0 cm^{-1}, at 100, 200, 500, 1000, 2000, 4000, and 8000 cm^{-1}.

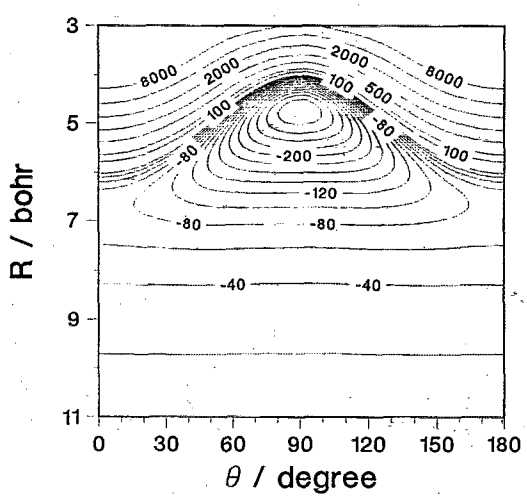

FIG. 3. Contour plot of the *adiabatic* potential energy surface of $N_2^+(A\,^2\Pi_{u,x})+He$; $r=2.11$ bohr. Lines are drawn every 20 cm^{-1} in the range from -280 to 0 cm^{-1}, at 100, 200, 500, 1000, 2000, 4000, and 8000 cm^{-1}.

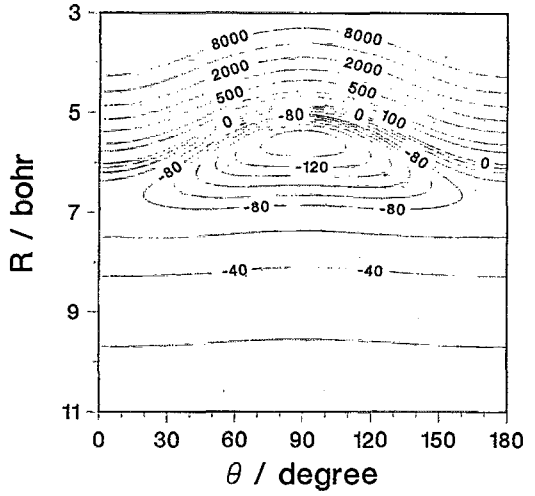

FIG. 4. Contour plot of the *adiabatic* potential energy surface of $N_2^+(A\,^2\Pi_{u,y})+He$; $r=2.11$ bohr. Lines are drawn every 10 cm^{-1} in the range from -130 to -80 cm^{-1}, every 20 cm^{-1} in the range from -80 to 0 cm^{-1}, at 100, 200, 500, 1000, 2000, 4000, and 8000 cm^{-1}.

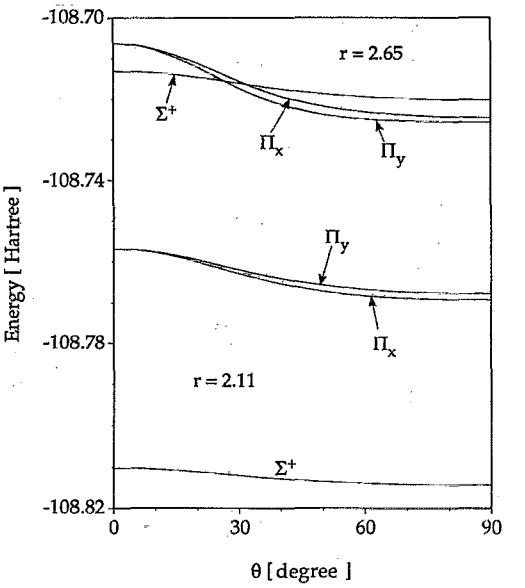

FIG. 5. *Diabatic* diagonal electronic matrix elements $\langle\Sigma^+|H_{el}|\Sigma^+\rangle$ and $\langle\Pi_{x,y}|H_{el}|\Pi_{x,y}\rangle$ as functions of the N_2^+–He angle θ for two different N_2^+ bond lengths r, and $R=4.8$ bohr.

diabatic potential energy surfaces as a function of θ. Figure 5 displays the angular dependence of the diagonal diabatic potentials $V_{\Pi_x}=V_\Pi-V_2$, $V_{\Pi_y}=V_\Pi+V_2$, and V_Σ for two different values of the N_2^+ bond length r. The potentials have been shifted by the computed asymptotic energies $T_\Sigma(r)$ and $T_\Pi(r)$, respectively. At $r=2.11$ bohr, the Σ and Π potentials are well separated due to the large difference of the energies $T_\Pi(2.11)$ and $T_\Sigma(2.11)$. With increasing N_2^+ distance, the potential energy functions $T_\Pi(r)$ and $T_\Sigma(r)$ of the isolated molecule approach each other (see Fig. 1) and cross at about $r=2.66$. As seen in Fig. 5, at $r=2.65$, $R=4.8$, and collinear geometries, the $^2\Pi$ state is still above the $^2\Sigma$ state. However, due to the smaller repulsion of the $^2\Pi$ potential at bent geometries, the diabatic potentials cross at about $\theta=30°$. In the adiabatic representations, this leads to an avoided crossing of the two A' states.

The splitting of the two $^2\Pi_u$ components due to the approach of the He atom is described by the V_2 potential, which is shown for various R's in Fig. 7. This splitting increases with increasing r, in particular, at intermediate angles. It becomes zero at collinear geometries and has two maxima at $\theta=45°$ and $\theta=135°$. The bimodal form as a function of the angle θ becomes more pronounced with increasing r. The V_1 coupling potential shown in Fig. 6 has a similar bimodal character. It is largest at about $\theta=30°$ and 150° and has a minimum at 90°. It is this V_1 potential which describes the nonadiabatic coupling between the $X\,^2\Sigma_g^+$ and $A\,^2\Pi_u$ states of the N_2^+ molecule. By symmetry, only odd terms in the angular expansion Eq. (11) of the V_1 potential contribute. As will be discussed in the next section, this leads to selection rules for the population of

TABLE V. Minima of the *diabatic* interaction potential energy surfaces[a] of the system N_2^+ + He for different bond distances r and angles θ.

		$\theta=0°$		$\theta=30°$		$\theta=60°$		$\theta=90°$	
State	r	R_{min}	$V(R_{min})$	R_{min}	$V(R_{min})$	R_{min}	$V(R_{min})$	R_{min}	$V(R_{min})$
	1.90	6.11	−133.36	5.92	−141.24	5.54	−154.57	5.38	−155.47
V_Σ[b]	2.11	6.17	−138.40	5.99	−142.34	5.65	−143.91	5.50	−138.80
	2.65	6.33	−148.35	6.22	−134.40	5.95	−110.50	5.76	−100.33
$V_\Sigma^{1,7}$[c]		6.22	−140.27	6.07	−138.62	5.73	−132.85	5.57	−127.17
	1.90	6.69	−74.14	6.31	−95.69	5.27	−197.04	4.55	−350.68
$V_{\Pi,x}$[b]	2.11	6.77	−74.85	6.39	−95.42	5.36	−187.71	4.69	−306.40
	2.65	6.97	−78.10	6.62	−91.39	5.62	−136.27	4.98	−188.45
$V_{\Pi,x}^{3,3}$[c]		6.86	−75.54	6.48	−93.77	5.43	−171.25	4.78	−264.32
	1.90	6.69	−74.14	6.41	−87.49	5.78	−125.80	5.49	−148.32
$V_{\Pi,y}$[b]	2.11	6.77	−74.85	6.49	−87.22	5.86	−120.16	5.58	−137.25
	2.65	6.97	−78.10	6.67	−87.00	6.01	−107.68	5.69	−114.59
$V_{\Pi,y}^{3,3}$[c]		6.86	−75.54	6.56	−86.82	5.92	−115.46	5.63	−128.97

[a] R_{min} and r given in bohr; $V(R_{min})$ is given in cm^{-1}.
[b] Potentials for different values of r as described in Eq. (13).
[c] Vibrationally adiabatic potentials as described in Eq. (14).

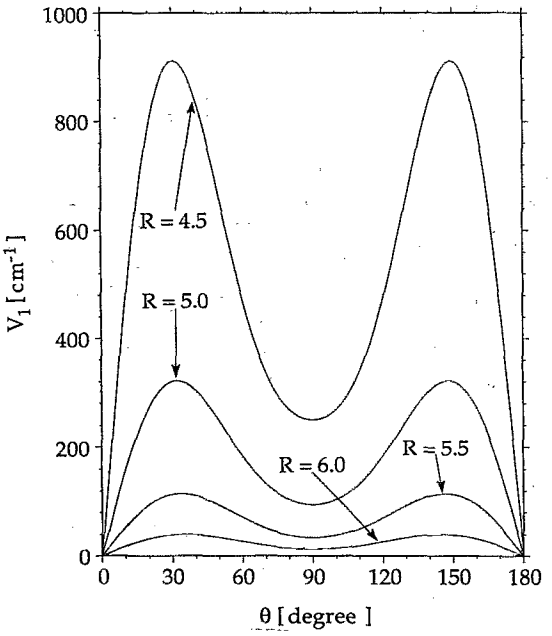

FIG. 6. *Diabatic* V_1 potential as a function of the N_2^+–He angle θ for different N_2^+–He distances R; r=2.11 bohr.

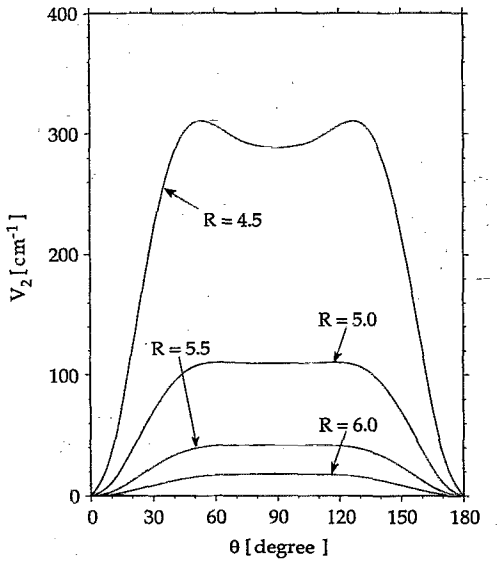

FIG. 7. *Diabatic* V_2 potential as a function of the N_2^+–He angle θ for different N_2^+–He distances R; r=2.11 bohr.

either only even or odd final rotational states. Both the V_1 and the V_2 potentials are smoothly varying with the N_2^+ bond distance r and decrease approximately exponentially with R.

IV. QUANTUM SCATTERING TREATMENT OF THE COLLISION DYNAMICS

As described in our earlier papers,[21,23] the total wave function of the isolated molecule can be written in a Hund's case (a) description[52,53] as a product of rotational, vibrational, and electronic wave functions, namely,

$$|JM\Omega\epsilon\Lambda\Sigma v\rangle = \frac{1}{\sqrt{2}}\left(|JM\Omega\rangle|\Lambda\Sigma\rangle + \epsilon|JM,-\Omega\rangle|-\Lambda,-\Sigma\rangle\right)|v\rangle, \qquad (15)$$

where J designates the total angular momentum with projections M and Ω along the space- and molecule-fixed axes, respectively. $|\Lambda\Sigma\rangle$ is the electronic wave function with projections Λ and Σ of the electronic orbital and spin-angular momentum along the molecular axis, and $|v\rangle$ denotes the vibrational wave function of the molecule with quantum number v. A $^2\Sigma^+$ state is characterized by $\Lambda=0$ and $\Sigma=\Omega=1/2$; a $^2\Pi_{1/2}$ is characterized state by $\Lambda=1$, $\Sigma=-1/2$ and $\Omega=1/2$; and finally a $^2\Pi_{3/2}$ state is characterized by $\Lambda=1$, $\Sigma=1/2$, and $\Omega=3/2$. The symmetry index ϵ in Eq. (15) can take the values ±1, and the total parity I of the molecular wave function is given by $\epsilon(-1)^{J-1/2}$.[54] For Π and Σ^+ states, the $\epsilon=+1$ levels are labeled e and the $\epsilon=-1$ levels f.[55] The vibronic wave functions of a homonuclear diatomic molecule are either symmetric (s) or antisymmetric (a) with respect to permutation of the identical nuclei. For *gerade* electronic states, levels with $I=+1$ have s symmetry and levels with $I=-1$ have a symmetry; this assignment is reversed for *ungerade* electronic states. The association of quantum numbers, indices, and labels to rotational levels are displayed in Table VI. A more complete presentation of assignments of ϵ, e/f, and parity to the molecular eigenstates can be found in Ref. 21.

TABLE VI. Assignment of quantum numbers, indices, and labels to rotational levels of a diatomic homonuclear molecule in $^2\Pi_u$ and $^2\Sigma_g^+$ electronic states.[a]

Total angular momentum[b]	$^2\Pi_u$ state					$^2\Sigma_g^+$ state			
	ϵ	e/f	I	s/a	N[c]	ϵ	e/f	I	s/a
$J+1$	+1	e	−	s	$J+1/2$	+1	e	−	a
	−1	f	+	a	$J+3/2$	−1	f	+	s
J	+1	e	+	a	$J-1/2$	+1	e	+	s
	−1	f	−	s	$J+1/2$	−1	f	−	a

[a]We assume a pure case (a) representation for the Π, and a case (b) representation of the Σ state.
[b]Without loss of generality, we assume $(J-1/2)$ is even.
[c]The value of the nuclear rotational angular momentum [the case (b) label].

The total Hamiltonian of the atom+molecule system can be written as

$$H(\mathbf{R},\mathbf{r}) = -\frac{\hbar^2}{2\mu R^2}\frac{d}{dR}\left(R^2\frac{d}{dR}\right) + \frac{L_{op}^2}{2\mu R^2} + H_{\mathrm{mol}}(\mathbf{r}) + V_{\mathrm{el}}(\mathbf{R},\mathbf{r}), \tag{16}$$

where the first two terms correspond, respectively, to the relative and orbital kinetic energies of the atom–molecule pair; the third term is the diatomic molecule Hamiltonian, which we shall assume to remain identical to the Hamiltonian of the isolated molecule, given in Table I of Ref. 23. The last term corresponds to the electrostatic interaction between the N_2^+ molecule and the helium atom, which vanishes at sufficiently large R and which was obtained in our *ab initio* calculations. The sum of H_{mol} and V_{el} is the total electronic Hamiltonian H_{el} which appears in Eqs. (6)–(8). The total wave function of the atom–diatom system is expanded in a set of eigenfunctions of the total angular momentum $\mathscr{J}$, which are defined by

$$|JL\Omega\epsilon\Lambda\Sigma v\mathscr{J}\mathscr{M}\rangle = \sum_{MM_L}(JML M_L|\mathscr{J}\mathscr{M}) \times |LM_L\rangle|JM\Omega\epsilon\Lambda\Sigma v\rangle, \tag{17}$$

where $(\cdots|\cdots)$ is a Clebsch–Gordan coefficient, $\mathscr{M}$ is the space-frame projection of $\mathscr{J}$, and $\mathbf{L}$ is the orbital angular momentum of the atom–molecule pair with space-frame projection M_L. Expressing the Schrödinger equation $(H-E)\cdot\Psi=0$ with the Hamiltonian of Eq. (16) in this *total angular momentum* basis yields the "close coupled" (CC) equations,[56] which are decoupled in $\mathscr{J}$ and $\mathscr{M}$.

The two kinetic energy terms in the total Hamiltonian are diagonal in the total $\mathscr{J}$ basis. The matrix elements of the molecular Hamiltonian H_{mol} have been given by Kotlar *et al.*[57] for $^2\Pi$ and $^2\Sigma^+$ states. H_{mol} is block diagonal in J, M, ϵ, and pairs (v_A,v_X) of neighboring $A\,^2\Pi_u$ and $X\,^2\Sigma_g^+$ vibrational levels. In our case, the 3×3 blocks further reduce to 2×2 blocks for the two $^2\Pi_u$ states and 1×1 blocks for the $^2\Sigma_g^+$ state, since there is no coupling between states of different permutation–inversion symmetry. Diagonalizing this molecular Hamiltonian for each combination of J, ϵ, and the pair (v_A,v_X) results in a set of three eigenstates ϕ_i, which are used as a basis in the scattering calculations. The index $i=1$, 2, and 3 denote the eigenstates in order of increasing energy eigenvalues. The eigenfunctions can be written as

$$|JM\phi_i\epsilon\rangle = \sum_{m=1}^{3} D_{im}|JM\Omega_m\epsilon\Lambda_m\Sigma_m v_m\rangle. \tag{18}$$

The coefficients D_{im} are assumed to be independent of R and θ. The matrix elements of the electrostatic coupling potentials in this $|JL\phi_i\epsilon\mathscr{J}\mathscr{M}\rangle$ basis are expanded as

$$V^{\mathscr{J}}_{J'L'\phi_i\epsilon',JL\phi_j\epsilon}(R) = \sum_{m,n=1}^{3} D^*_{im}D_{jn}V^{\mathscr{J}}_{J'L'\Omega_m\epsilon'\Lambda_m v_m,JL\Omega_n\epsilon\Lambda_n v_n}(R). \tag{19}$$

Here and in the following, we have omitted the indices Σ_m, Σ_n, which are equal to $\frac{1}{2}$ in each case. The potential matrix elements in the $|JM\Omega_i\epsilon\Lambda v\rangle$ basis are given by

$$V^{\mathscr{J}}_{J'L'\Omega_m\epsilon'\Lambda_m v_m,JL\Omega_n\epsilon\Lambda_n v_n}(R) = (-1)^{\mathscr{J}+J+J'-\Omega}[(2J+1)(2J'+1)(2L+1)(2L'+1)]^{1/2}\sum_l \begin{pmatrix} L' & l & L \\ 0 & 0 & 0\end{pmatrix} \times \begin{Bmatrix} J' & L' & \mathscr{J} \\ L & J & l\end{Bmatrix}\frac{1}{2}[1-\epsilon\epsilon'(-1)^{J+J'+l}]V_l(J'\Omega_m\epsilon'\Lambda_m v_m,J\Omega_n\epsilon\Lambda_n v_n;R). \tag{20}$$

The explicit forms for the V_l matrix elements can be found in Refs. 21 and 23.

To solve the close-coupled equations, the total wave function of the system is propagated into the asymptotic region,[58–60] where the S and T matrices can be obtained by standard procedures.[56] The cross sections for inelastic transitions are then calculated from the scattering T matrices. A practical disadvantage of CC calculations arises from the fact that the computational effort scales as N^3, with N being the number of coupled channels. The number of coupled channels in a CC calculation is roughly equal to $j_{\max}^2$, where $j_{\max}$ is the maximum rotational quantum number included in the expansion of the scattering wave function in Eq. (17). Thus the overall numerical effort scales with $j_{\max}^6$. Replacing the centrifugal terms in the CC equations by an average centrifugal term $\hbar^2\bar{L}(\bar{L}+1)/2\mu R^2$ decouples the rotational and orbital angular momenta, and the potential matrix can be block diagonalized. The number of coupled channels within this "coupled-states" (CS) approximation[61] is considerably reduced, and the overall computational effort is only roughly $2j_{\max}^4$ which leads to significant savings of central processing unit (CPU) time.

In the particular case of collisions involving homonuclear diatomic molecules, where the two electronics under consideration have opposite permutation–inversion symmetry, only *odd* l terms contribute to the V_l potential. Together with the phase factor $\frac{1}{2}[1-\epsilon\epsilon'(-1)^{J+J'+l}]$ in Eq. (20), this implies that coupling between Π and Σ levels will be nonzero only if the two levels have *opposite* parity $[\epsilon(-1)^{J-1/2}]$.[54] According to the assignment of symmetry labels in Table VI, this means that only those inelastic transitions are allowed which conserve the *s/a* symmetry.

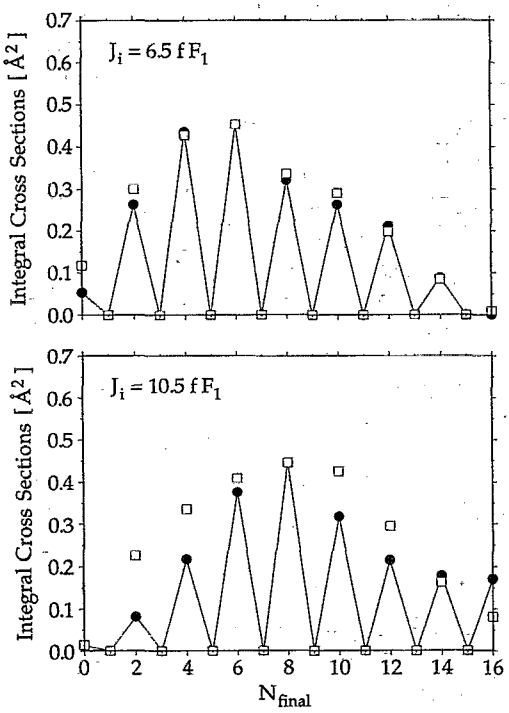

FIG. 8. A comparison of theoretical and experimental cross sections for transitions between $A,v=4,JfF_1$ and $X,v'=8,N'$. Filled circles connected by solid lines denote calculated cross sections at $E_{tr}=511$ cm^{-1}, and open squares denote experimental intensities scaled to the highest calculated cross section. The initial states are $J=6.5fF_1$ (upper panel) and $J=10.5fF_1$ (lower panel).

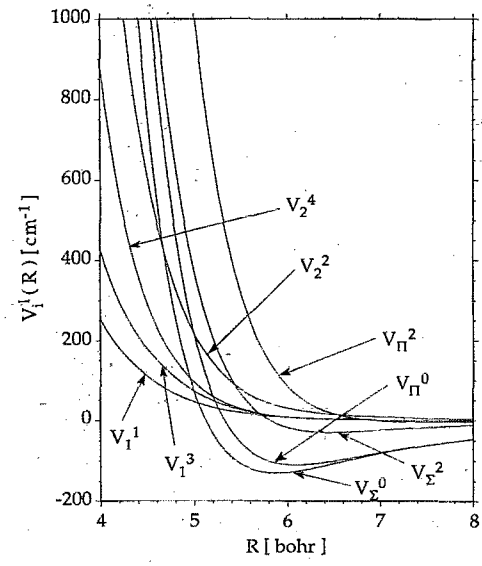

FIG. 9. V_l^i terms of the *diabatic* interaction potential expansion as a function of the N_2^+–He distance R.

The assignment of the s/a labels to the e and f Λ doublets of the $^2\Pi_u$ and to the N levels of the $^2\Sigma_g^+$ state is summarized in Table VI.

V. RESULTS AND DISCUSSION

All scattering calculations were performed with the HIBRIDON code.[62] To obtain converged cross sections, it was necessary to include all energetically open and several closed fine-structure levels of the $^2\Pi_{u,1/2}$, $^2\Pi_{u,3/2}$, and $^2\Sigma_g^+$ states. The relative rotational energies were obtained from known spectroscopic constants.[50,63] All results presented below were obtained within the CS approximation, since comparisons with a number of full CC calculations showed that cross sections for both levels of theory were in good agreement. This is in line with what we found in the CN+He system.[15] In the following calculations, we used the vibrationally averaged potentials as described in Sec. III.

To compare theoretically calculated and experimentally measured cross sections, we first focus on transitions out of the $A,v=4,J=6.5fF_1$ and $A,v=4,J=10.5fF_1$ levels into the $X,v=8,N'$ rotational manifold, as studied experimentally by Katayama *et al.*[5] The cross sections were summed over the final state spin doublets, which were not resolved in most experiments. The results of our scattering calculations for a collision energy of 511 cm^{-1} are plotted in Fig. 8. The collision energy of 511 cm^{-1} is larger than the most probable collision energy at room temperature (311 cm^{-1}). We chose the former value to simulate the broad experimental velocity distribution. In particular, transitions were observed experimentally into high final J states which are energetically closed at a collision energy of 311 cm^{-1}. A more rigorous treatment would be to perform scattering calculations for a large variety of collision energies and weigh the obtained cross sections with the probabilities of a Maxwell–Boltzmann velocity distribution. The experimental intensities were scaled to match the largest computed electronically inelastic transition. In agreement with experiment, transitions with $\Delta J\approx 0$ are largest, and the cross sections decrease with increasing ΔJ. This effect can be explained by the dominance of the $l=1$ and $l=3$ terms in the angular expansion of the V_1 potential (Fig. 9). In first order, a term of given l can couple only states with $\Delta J\leqslant l$. In general, the experimental X state rotational distributions are somewhat broader than the theoretically calculated ones, which might be due to multiple collision effects[15] or deficiencies in the angular dependence of the calculated V_1 potential for higher values of l.

A general feature of the calculated and experimental cross sections is that transitions with different *permutation–inversion* symmetry for initial and final rotational states vanish. In other words, only every second final state level N is populated. The phase of this alternation changes with the Λ doublet index e/f and quantum number J of the initial state. This is demonstrated in Fig. 10, where cross sections for scattering out of $A,v=3,J=6.5$ (upper panel) and $A,v=3,J=5.5$ (lower panel) into $X,v'=7,N'$ are plotted, respectively. For *even* rotational quantum number, $J-1/2$ transitions out of the $f(e)$ Λ doublet are only allowed into *even(odd)* final N' states. For *odd* $J-1/2$, this occupancy pattern is reversed. This selection rule is a reflection of the permutation–inversion symmetry of the N_2^+ moiety, and the consequent vanishing of all even-l terms in the expansion of the V_1 coupling poten-

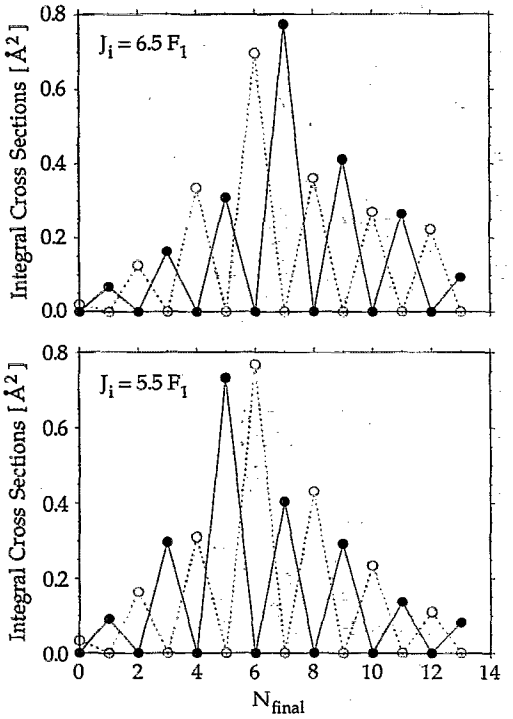

FIG. 10. Cross sections for transitions from $A,v=3,J=6.5fF_1\rightarrow X,v'=7,N'$ (upper panel) and $A,v=3,J=5.5F_1\rightarrow X,v'=7,N'$ (lower panel) at a translational energy of 311 cm^{-1}. Transitions out of symmetric Λ doublet states are designated by open circles connected by dashed lines; transitions out of antisymmetric Λ doublet states are designated by filled circles connected by solid lines.

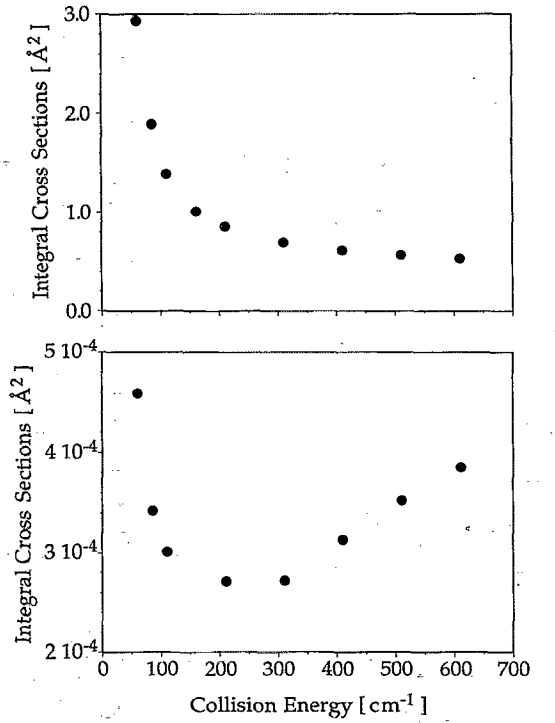

FIG. 11. Cross sections for $\Delta J=0$ transitions from $A,v=3,J=6.5fF_1\rightarrow X,v'=7,N'$ (upper panel) and $A,v=4,J=6.5fF_1\rightarrow X,v'=7,N'$ (lower panel) at different collision energies.

tial, as discussed above in Sec. IV. Notice that in all cases, the propensity $\Delta J\approx 0$ is valid.

Katayama and co-workers found in their experiments that cross sections increase with decreasing collision energy.[10] To investigate this feature, which has also been seen for the system $CO^+ + He$,[4] we performed scattering calculations for the transitions $A,v=3,J=6.5fF_1\rightarrow X,v'=7$ (small energy gap) and $A,v=4,J=6.5fF_1\rightarrow X,v'=7$ (large energy gap) at different collision energies. The results are displayed in Fig. 11, where we plot the cross sections for $\Delta J=0$ transitions at different collision energies. Decreasing the collision energy from the room temperature value leads for both small and large gap transitions to enlarged cross sections. It is likely that this behavior is due to the potential well, since for lower energies, the He atom can remain longer in the attractive region of the interaction potential, thus leading to enlarged cross sections. However, increasing the collision energy to higher than thermal energy also leads to an increase of the electronically inelastic cross sections for transitions traversing large energy gaps. With higher translational energy, the classical turning point of the He atom is shifted to smaller R distances where the V_1 coupling potential becomes larger. These two competitive effects lead to a minimum in the energy dependence of the cross sections for large energy gap transitions. The $\Delta J=0$ cross sections for nearly isoenergetic transitions are continuously decreasing with increasing collision energy. The higher the collision energy, the more rotational levels are energetically open, and so the total flux distributes over a larger number of channels.

Up to this point, the cross sections from our scattering calculations have been summed over the final state spin doublets to compare with the bulk of experimental data. In recent experiments, Katayama and co-workers[10] obtained final state resolved cross sections by utilizing perturbative effects of rotational levels in the $B\,^2\Sigma_u^+, v=5$ state. Their observation of a propensity $f\rightarrow f$ for $\Delta J<0$ transitions from the F_1 spin–orbit manifold and $f\rightarrow e$ for transitions from the F_2 manifold is reproduced quite well by our calculations (Fig. 12). This result is in line with the predictions of Alexander and Corey[21] that ϵ-conserving transitions ($f\rightarrow f$, $e\rightarrow e$) are more probable out of the F_1 than out of the F_2 manifold. A numerical proof of the validity of this propensity is given in the lowest panel of Fig. 12, where we compare cross sections for transfer into the X-state spin doublets from the F_1 spin–orbit manifold to those from the F_2 manifold. In the high J limit, this ratio is expected to converge to unity both for ϵ-conserving and ϵ-changing transitions. A shift of this propensity to conserve the parity towards a preference of parity-changing transitions from the F_1 component for high J_{final} is not observable theoretically. Moreover, it seems that in the high J limit, transitions into f final states are preferred no matter whether the initial state belonged to the F_1 or F_2 manifold.

In Fig. 13, we compare cross sections for spin–orbit conserving and spin–orbit changing $A\rightarrow A$ rotationally inelastic with electronically inelastic $A\rightarrow X$ transitions within

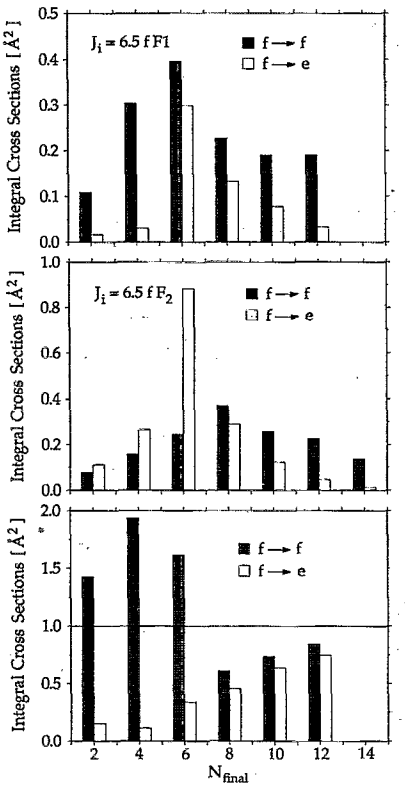

FIG. 12. Final state spin doublet resolved cross sections for scattering out of $A,v=3,J=6.5fF_1(F_2)$ into $X,v'=7,N'$. (Uppermost panel) Scattering out of the F_1 spin–orbit manifold. (Middle panel) Scattering out of the F_2 spin–orbit manifold. The final state e spin components are indicated by empty bars; f components are indicated by filled bars. (Lowest panel) Ratio of the cross sections for the $A,v=3,J=6.5fF_1\rightarrow X,v'=7,J'$ transition as compared to those for the $A,v=3,J=6.5fF_2\rightarrow X,v'=7,J'$ transitions as a function of the final rotational quantum number N'. The ϵ-conserving transitions are indicated by filled bars; ϵ-changing transitions are indicated by empty bars.

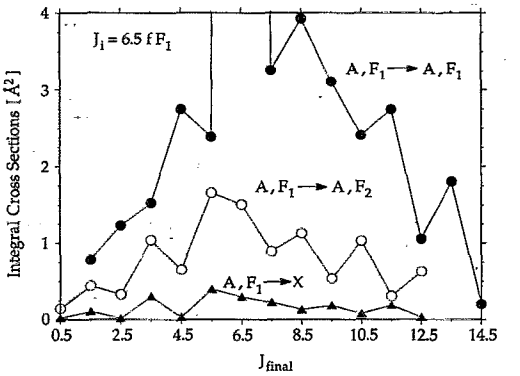

FIG. 13. A comparison of $A,J=6.5fF_1\rightarrow A,J'F_1$, $A,J=6.5fF_1\rightarrow A,J'F_2$, and $A,J=6.5fF_1\rightarrow X,J'$ cross sections between $v_A=3$ and $v_X=7$ vibrational states. Spin–orbit conserving transitions are indicated by filled circles; spin–orbit changing transitions are indicated by open circles. Filled triangles denote electronically inelastic transitions.

the $v_A=3$ and $v_X=7$ vibrational states of the N_2^+ + He system. It can be seen that pure rotational energy transfer $F_1\rightarrow F_1$ is the most effective relaxation path for the initially excited rotational state, whereas spin–orbit changing ($F_1\rightarrow F_2$) transitions are about two to three times less probable. This is very similar to what we found in the CN + He system.[15] Electronic energy transfer is about ten times less probable than spin–orbit conserving rotationally inelastic transitions.

So far, we have only considered electronically inelastic transitions between vibrational levels with small energy gaps. As mentioned before, also transitions to the next lower vibrational levels, which are separated from the initial levels by energy gaps of about 2000 cm^{-1}, have been observed experimentally. For these "off-resonance" transitions, our calculated cross sections are in general very small (see the lower panel of Fig. 11). This result is in line with our studies for the system CN + He,[23] but in striking disagreement with the experimental findings. One possible source of error is the neglect of vibrational coupling in our previous scattering calculations. We therefore performed a systematic study of vibrational effects, which is presented below.

In a first set of calculations, we investigated the effect of vibrational averaging the four diabatic potential energy surfaces. We calculated cross sections for the transitions $A,v=3(4),J=6.5fF_1\rightarrow X,v'=7,N'$ with two different interaction potentials. First we used the potentials for the N_2^+ bond distance fixed at $r=2.11$ bohr, which is near the equilibrium geometry of the $X\,^2\Sigma_g^+$ state ($r_e=2.1097$ bohr). The coupling potential $V_1(R,\theta,r=2.11)$ was multiplied by the appropriate overlap matrix elements $\langle v|v'\rangle$. We denote this method, which has also been used in our previous calculations for CN + He, as the "rigid rotor, Franck–Condon approximation." The second calculation was performed with the vibrationally averaged potentials as described in Sec. III. Since in the energetically accessible region the coupling matrix elements $\langle v|V_\Lambda(R,\theta,r)|v'\rangle$, where $\Lambda=\Sigma$ or Π, are small as compared to the vibrational spacings, these potentials are virtually identical to "vibrationally adiabatic potentials," which are obtained by diagonalizing the matrices $\langle v|T_\Lambda+V_\Lambda(R,\theta,r)|v'\rangle$. Correspondingly, we denote this method as the "vibrationally adiabatic approximation."

A comparison of results for both approximations is displayed in Fig. 14. In the case of the small energy gap transitions, the magnitude of the cross sections for transitions with $\Delta J\neq 0$ is hardly influenced, but it is substantially increased for $\Delta J=0$ when the vibrationally adiabatic potentials are used. This leads to a more pronounced propensity to minimize ΔJ. Moreover, using the vibrationally averaged potentials leads to a *decrease* of the cross sections for large energy gap transitions as compared to the rigid rotor approximation. Similar effects are found for the transitions $A,v=3\rightarrow X,v'=6$ and $A,v=4\rightarrow X,v'=8$. This effect originates from the different r dependence of the interaction potentials for the $X\,^2\Sigma_g^+$ and $A\,^2\Pi_u$ states, which leads to shifts of the effective energetic positions of the vibrational states during the collision. This is illustrated in Fig. 15, which shows the V_Σ–V_Π splitting as a function of the N_2^+–He distance R for the rigid rotor and vibrationally adiabatic potentials, respectively. For $\theta=0°$, the splitting is negative, which means that with the approach of the per-

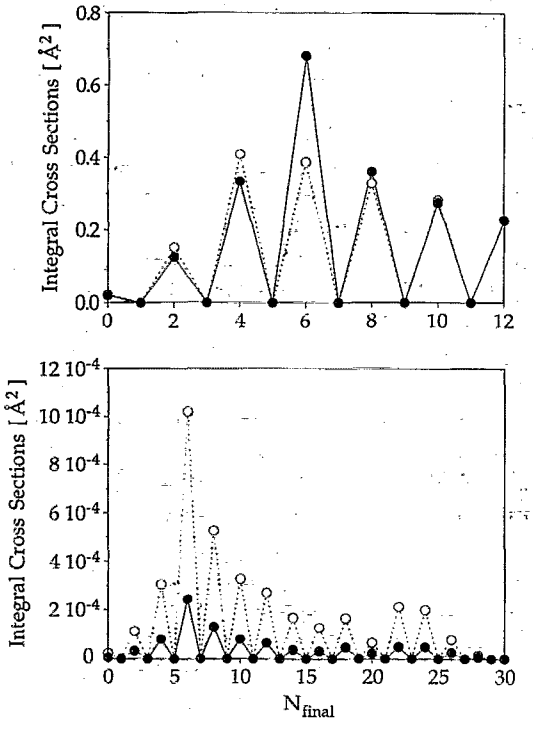

FIG. 14. Cross sections for the transition $A,v=3(4),J=6.5fF_1 \rightarrow X,v'=7$ as a function of the case (b) rotational quantum number N. The translational energy is 311 cm^{-1} for all calculations. Open circles connected by dashed lines denote cross sections calculated within the "rigid-rotor approximation." Filled circles connected by solid lines denote cross sections for the "vibrationally adiabatic approximation." (Upper panel) Scattering out of $v_A=3$. (Lower panel) Scattering out of $v_A=4$.

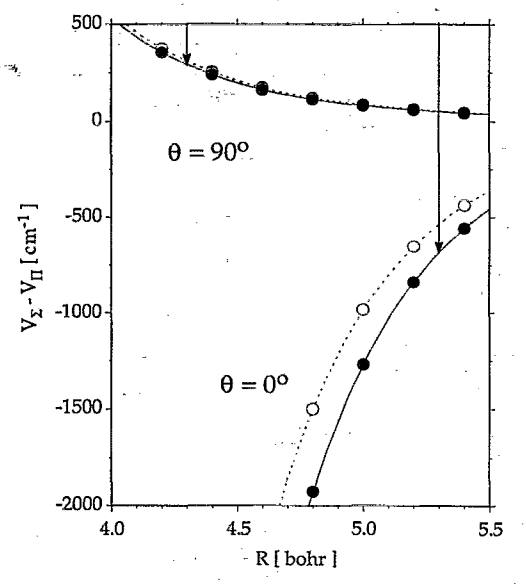

FIG. 15. The difference between the *diabatic* V_Σ and V_Π potentials as a function of the distance R for a fixed N_2^+ bond distance and two angles θ. Open circles connected by dashed lines denote the splitting of V_Σ and V_Π within the rigid-rotor approximation. Filled circles connected by solid lines denote the V_Σ–V_Π splitting within the vibrationally adiabatic approximation. The arrows denote the classical turning points for room temperature collisions (311 cm^{-1}) for each angle θ.

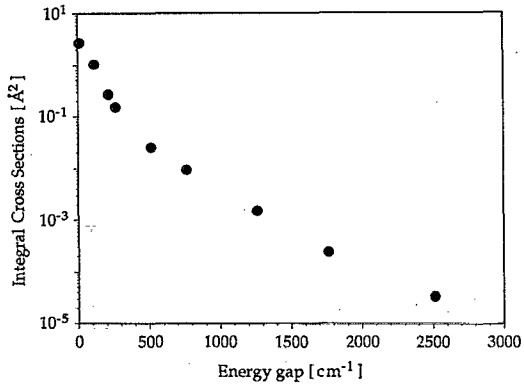

FIG. 16. Cross sections for the transition $A,v=4,J=6.5fF_1 \rightarrow X,v'=7,N'=6$, where the energy gap between the vibrational states has artificially been varied. The correct energy gap is about 1760 cm^{-1}. The translational energy is 311 cm^{-1}.

turber, the energy gap between the vibrational states becomes larger. At the classical turning point for room temperature collisions ($R_{ctp}=5.3$ bohr at collinear geometry), this additional splitting amounts to about 540 and 680 cm^{-1} for the rigid rotor and vibrationally adiabatic approximations, respectively. For the perpendicular approach ($\theta=90°$, $R_{ctp}=4.3$ bohr), the vibrational states move closer together, but the difference between the rigid rotor and vibrationally adiabatic potentials is much smaller than for collinear geometries.

In order to investigate the energy-gap sensitivity more directly, we performed some scattering calculations in which the energy gap between the $v_A=4$ and $v_X=7$ vibrational states was artificially varied by shifting the asymptotic energy of the vibrational levels. In Fig. 16, we plotted the cross sections for the $\Delta J=0$ transition for $A,v=4,J=6.5fF_1$ to $X,v'=7,N'=6$ on a logarithmic scale vs the magnitude of the energy gap. The "real" energy gap is about 1760 cm^{-1} for this transition. Making the energy gap smaller by 500 cm^{-1} leads to an increase of cross sections by about one order of magnitude. In order to remove the discrepancy between theory and experiment, an energy shift of more than 1000 cm^{-1} would be necessary. It is very unlikely that the error in the relative energies of our potential energy surfaces is so large.

In a third set of calculations, we studied the effect of vibrational coupling between vibrational levels of the same electronic state. The coupling is described by the off-diagonal matrix elements $\langle v | V_\Lambda(R,\theta,r) | v' \rangle$, which were neglected in the rigid rotor and vibrationally adiabatic approximations described above. Since the computational effort increases dramatically with increasing number of vibrational states, we were not able to study directly the convergence of our results with respect to the number of vibrational states included. However, we found that in the eigenvectors of the matrices $\langle v | T_\Lambda + V_\Lambda(R,\theta,r) | v' \rangle$ (for fixed R, θ), only vibrational states differing by $\Delta v = \pm 1$ had significant coefficients. Therefore, we included only the neighboring vibrational states of the pair under investigation in our scattering calculations. In Fig. 17, we compare

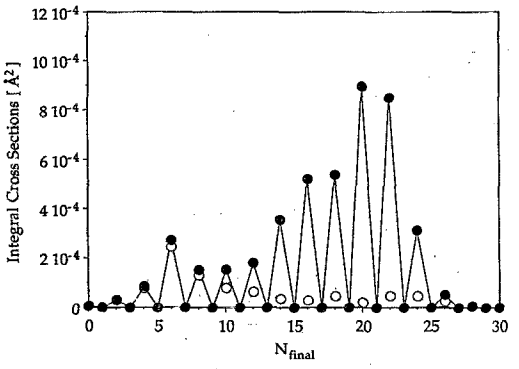

FIG. 17. Cross sections for transitions $A,v=4,J=6.5fF_1 \rightarrow X,v'=7,N'$ at a translational energy of 311 cm^{-1}. Open circles denote cross sections calculated with only the $v_A=4$ and $v_X=7$ rotational levels included in the channel basis. Filled circles connected by solid lines denote cross sections calculated with additional rotational levels of the $v_A=3$, $v_X=6$ and $v_X=8$ vibrational manifolds included in the channel basis.

transitions from the initial level $A,v=4,J=6.5fF_1$ into the $X,v'=7$ rotational manifold for calculations with the (4|7) and (3,4|6,7,8) vibrational levels included. It is found that the vibrational coupling slightly increases the cross sections for $\Delta J \approx 0$ transitions. However, this effect is by far too small to explain the experimentally observed line intensities for transitions that traverse large energy gaps. Various other combinations of vibrational states have also been tested, but neither of them lead to larger effects.

Interestingly, the probability of transitions into final states with high N' is dramatically increased, an effect which has not yet been seen experimentally. It can be explained as follows: The initial rotational state of the $v_A=4$ manifold is coupled to high J states of the $v_A=3$ manifold by nondiagonal $V_\Pi(v,v')$ matrix elements. These states are nearly isoenergetic to the final high N' states of the $v_X=7$ manifold to which they are coupled by the V_1 potential. The magnitude of cross sections for these transitions is comparable to cross sections for rotational–vibrational transfer processes within a single electronic state.

VI. SUMMARY

Accurate three-dimensional potential energy surfaces for the three lowest electronic states of $N_2^+ + He$ have been computed using large scale multireference configuration expansions. The adiabatic potentials resulting from the *ab initio* calculations have been transformed to a diabatic representation, in which a fourth potential describing the collision-induced nonadiabatic coupling of the two A' states appears. The four diabatic potentials were fitted to analytical functions, vibrationally averaged, and subsequently used in quantum scattering calculations of cross sections for rotationally, vibrationally, and electronically inelastic transitions within and between the $A\,^2\Pi_u$ and $X\,^2\Sigma_g^+$ rovibrational manifolds of N_2^+.

In general, good agreement between calculated and experimental cross sections is found for electronically inelastic transitions with small energy gaps. However, the computed cross sections for transitions between vibrational levels which are separated by 1750–2000 cm^{-1} appear to be three orders of magnitude smaller than the experimental ones. This is due to an approximately exponential decrease of the calculated cross sections with increasing energy gap. Attempts to resolve this discrepancy by including vibrational couplings into the scattering calculations were not successful. Hence, the discrepancy between experiment and the present calculations remains further unresolved. We note that Heaven recently studied vibrational and electronic predissociation of the $CN(A\,^2\Pi_{1/2},v=3)+Ne$ van der Waals complex.[64] He found that predissociation via electronic transitions to the $CN(X\,^2\Sigma^+,v=7)$ level, which in our treatment are induced by the V_1 potential, is several orders of magnitude slower than via transitions to the $CN(A\,^2\Pi_{3/2},v=3)+Ne$ states, which are induced by the V_2 potential. This is in full accord with our theoretical predictions for the relative cross sections. In the bound state experiments of Heaven, only the well region of the potential is tested. Consequently, the discrepancies between the present calculated cross sections and the experimental measurements of Katayama and co-workers might be due to errors in the description of the dynamics in the short-range, repulsive region. Possible mechanisms involve collision-induced changes of the spin–orbit coupling in the diatomic molecule or in the neglected off-diagonal elements of the electronic orbital (L^2) operator in Eq. (16). Such effects will be subject of future investigations in our laboratory.

ACKNOWLEDGMENTS

The *ab initio* as well as scattering calculations reported in this paper were performed on the Cray YMP832 of the Höchstleistungsrechenzentrum Jülich, Germany. We wish to thank the Deutsche Forschungsgemeinschaft (SFB216), and the Deutsche Fonds der Chemischen Industrie for support of this work. We are also grateful to Millard Alexander for providing his HIBRIDON scattering code and many helpful discussions.

[1] V. E. Bondybey and T. A. Miller, J. Chem. Phys. **69**, 3597 (1978).
[2] D. H. Katayama, T. A. Miller, and V. E. Bondybey, J. Chem. Phys. **71**, 1662 (1979).
[3] D. H. Katayama, T. A. Miller, and V. E. Bondybey, J. Chem. Phys. **72**, 5469 (1980).
[4] D. H. Katayama and J. A. Welsh, Chem. Phys. Lett. **106**, 74 (1984).
[5] D. H. Katayama, J. Chem. Phys. **81**, 3495 (1984).
[6] D. H. Katayama, Phys. Rev. Lett. **54**, 657 (1985).
[7] D. H. Katayama and A. V. Dentamaro, J. Chem. Phys. **85**, 2595 (1986).
[8] D. H. Katayama, A. V. Dentamaro, and J. A. Welsh, J. Chem. Phys. **87**, 6983 (1987).
[9] D. H. Katayama and A. V. Dentamaro, J. Chem. Phys. **91**, 4571 (1989).
[10] A. V. Dentamaro and D. H. Katayama, Phys. Rev. A **43**, 1306 (1991).
[11] N. Furio, A. Ali, and P. J. Dagdigian, Chem. Phys. Lett. **125**, 561 (1986).
[12] N. Furio, A. Ali, and P. J. Dagdigian, J. Chem. Phys. **85**, 3860 (1986).
[13] Guo Jihua, A. Ali, and P. J. Dagdigian, J. Chem. Phys. **85**, 7098 (1986).
[14] A. Ali, Guo Jihua, and P. J. Dagdigian, J. Chem. Phys. **87**, 2045 (1987).
[15] P. J. Dagdigian, D. Patel-Misra, A. Berning, H.-J. Werner, and M. H. Alexander, J. Chem. Phys. **98**, 8580 (1993).
[16] W. M. Gelbart and K. F. Freed, Chem. Phys. Lett. **18**, 470 (1973).

[17] R. W. Field, C. R. Jones, and H. P. Broida, J. Chem. Phys. **60**, 4377 (1974).
[18] M. H. Alexander, J. Chem. Phys. **76**, 3637 (1982).
[19] M. H. Alexander and M. Osmolovsky, J. Chem. Phys. **77**, 839 (1982).
[20] H. Lefebvre-Brion and R. W. Field, *Perturbations in the Spectra of Diatomic Molecules* (Academic, New York, 1986).
[21] M. H. Alexander and G. C. Corey, J. Chem. Phys. **84**, 100 (1986).
[22] H.-J. Werner, B. Follmeg, and M. H. Alexander, J. Chem. Phys. **89**, 3139 (1988).
[23] H.-J. Werner, B. Follmeg, M. H. Alexander, and D. Lemoine, J. Chem. Phys. **91**, 5425 (1989).
[24] MOLPRO is a suite of *ab initio* programs written by H.-J. Werner and P. J. Knowles with contributions by J. Almlöf, R. D. Amos, S. T. Elbert, W. Meyer, E.-A. Reinsch, R. M. Pitzer, A. J. Stone, and P. R. Taylor.
[25] S. Huzinaga, J. Chem. Phys. **42**, 1293 (1965).
[26] S. Huzinaga, internal report, Department of Chemistry, University of Alberta, 1965.
[27] F. B. van Duijneveldt, IBM research report RJ 945, internal report, IBM, 1971.
[28] A. D. Buckingham, Adv. Chem. Phys. **12**, 107 (1967).
[29] W. Meyer, Int. J. Quantum Chem. Symp. **5**, 341 (1971).
[30] W. Meyer, J. Chem. Phys. **58**, 1017 (1973).
[31] A. J. Thakkar, J. Chem. Phys. **75**, 4496 (1981).
[32] C. R. Mansfield and E. R. Peck, J. Opt. Soc. Am. **59**, 199 (1976).
[33] K. A. Peterson, R. A. Kendall, and T. H. Dunning, Jr., J. Chem. Phys. **99**, 1930 (1993).
[34] H.-J. Werner and W. Meyer, J. Chem. Phys. **73**, 2342 (1980).
[35] H.-J. Werner and W. Meyer, J. Chem. Phys. **74**, 5794 (1981).
[36] H.-J. Werner and P. J. Knowles, J. Chem. Phys. **82**, 5053 (1985).
[37] P. J. Knowles and H.-J. Werner, Chem. Phys. Lett. **115**, 259 (1985).
[38] H.-J. Werner and P. J. Knowles, J. Chem. Phys. **89**, 5803 (1988).
[39] P. J. Knowles and H.-J. Werner, Chem. Phys. Lett. **145**, 514 (1988).
[40] P. J. Knowles and H.-J. Werner, Theor. Chim. Acta **84**, 95 (1992).
[41] S. F. Boys and F. Bernardi, Mol. Phys. **19**, 553 (1970).
[42] W. Meyer, P. C. Hariharan, and W. Kutzelnigg, J. Chem. Phys. **73**, 1880 (1980).
[43] S. R. Langhoff and E. R. Davidson, Int. J. Quantum Chem. **8**, 61 (1974).
[44] R. J. Gdanitz and R. Ahlrichs, Chem. Phys. Lett. **154**, 413 (1988).
[45] H.-J. Werner and P. J. Knowles, Theor. Chim. Acta **78**, 175 (1990).
[46] A. Degli Esposti and H.-J. Werner, J. Chem. Phys. **93**, 3351 (1990).
[47] A. Jörg, A. Degli Esposti, and H.-J. Werner, J. Chem. Phys. **93**, 8757 (1990).
[48] D. M. Brink and G. R. Satchler, *Angular Momentum* (Clarendon, Oxford, 1968).
[49] K. P. Huber and G. Herzberg, *Constants of Diatomic Molecules* (Van Nostrand, Princeton, 1979).
[50] A. Lofthus and P. H. Krupenie, J. Phys. Chem. Ref. Data **6**, 113 (1977).
[51] J. W. Cooley, Math. Comput. **15**, 363 (1961).
[52] G. Herzberg, *Spectra of Diatomic Molecules* (Van Nostrand, Princeton, 1968).
[53] R. N. Zare, A. L. Schmeltekopf, W. J. Harrop, and D. L. Albritton, J. Mol. Spectrosc. **46**, 37 (1973).
[54] M. Larsson, Phys. Scr. **23**, 835 (1981).
[55] J. M. Brown, J. T. Hougen, K. P. Huber, J. W. C. Johns, I. Kopp, H. Lefebvre-Brion, A. R. Merer, D. A. Ramsay, J. Rostas, and R. N. Zare, J. Mol. Spectrosc. **55**, 500 (1975).
[56] D. Secrest, *Atom–Molecule Collision Theory: A Guide for the Experimentalist* (Plenum, New York, 1979).
[57] A. J. Kotlar, R. W. Field, J. I. Steinfield, and J. A. Coxon, J. Mol. Spectrosc. **80**, 82 (1980).
[58] M. H. Alexander, J. Chem. Phys. **81**, 4510 (1984).
[59] D. E. Manolopoulos, J. Chem. Phys. **85**, 6425 (1986).
[60] M. H. Alexander and D. E. Manolopoulos, J. Chem. Phys. **86**, 2044 (1987).
[61] P. McGuire and D. J. Kouri, J. Chem. Phys. **60**, 2488 (1974).
[62] HIBRIDON is a package of programs for the time-independent quantum treatment of ineleastic collisions and photodissociation written by M. H. Alexander, D. E. Manolopoulos, H.-J. Werner, and B. Follmeg, with contributions by P. F. Vohralik, D. Lemoine, G. Corey, B. Johnson, T. Orlikowski, W. Kearney, A. Berning, A. Degli-Esposti, C. Rist, and P. Dagdigian.
[63] T. A. Miller, T. Suzuki, and E. Hirota, J. Chem. Phys. **80**, 4671 (1984).
[64] M. C. Heaven, presented at the conference on the Dynamics of Molecular Collisions, June 1993, Helen, Georgia.